Uncertainties in NLO + parton shower matched simulations of inclusive jet and dijet production

Stefan Höche[1], Marek Schönherr[2]

[1] SLAC National Accelerator Laboratory, Menlo Park, CA 94025, USA
[2] Institute for Particle Physics Phenomenology, Durham University, Durham DH1 3LE, UK

Abstract: We quantify uncertainties in the Monte-Carlo simulation of inclusive and dijet final states, which arise from using the MC@NLO technique for matching next-to-leading order parton level calculations and parton showers. We analyse a large variety of data from early measurements at the LHC. In regions of phase space where Sudakov logarithms dominate over high-energy effects, we observe that the main uncertainty can be ascribed to the free parameters of the parton shower. In complementary regions, the main uncertainty stems from the considerable freedom in the simulation of underlying events.

1 Introduction

QCD jet production constitutes an important background in a variety of searches for theories beyond the Standard Model [1–6]. At the same time, measurements of inclusive jet and dijet cross sections are used to constrain parton distributions [7–9] and to determine the value of the strong coupling [10–12]. Despite the tremendous importance of QCD jet production, precise predictions of event rates and kinematics using higher-order perturbation theory remain challenging. Only up to four-jet final states have been computed at the next-to-leading order so far [13–20]. Phenomenologists therefore typically rely on the simulation of high-multiplicity signatures by Monte-Carlo event generators.

The ATLAS and CMS experiments at the CERN Large Hadron Collider have recently measured inclusive jet and dijet production [21–27], with many observables implicitly probing higher-order effects. The outstanding quality of these data allows to validate and refine existing Monte-Carlo tools. The scope of this publication is a quantification of related perturbative and non-perturbative uncertainties.

Calculating next-to-leading order QCD corrections to arbitrary processes has become a highly automated procedure, limited only by the capacity of contemporary computing resources. Infrared subtraction techniques [28–30] are implemented by several general-purpose matrix element generators [31–35]. The computation of virtual corrections is tackled by a variety of dedicated programs [36–51]. Turning the parton level result into a prediction at the particle level then requires a matching to the parton shower in order to implement resummation. Two methods have been devised to perform this matching procedure, the MC@NLO [52] and the POWHEG [53, 54] technique. While both are formally correct at the next-to-leading order, they

exhibit subtle differences, which have been in the focus of interest recently [55,56]. We shall continue this study to some extent and perform a detailed comparison of scale uncertainties with resummation uncertainties as well as ambiguities arising from the Monte-Carlo simulation of the underlying event. We will employ the MC@NLO technique to match next-to-leading order parton-level results for dijet production with the parton shower as implemented in the event generator SHERPA [57,58]. Virtual corrections are obtained from the BLACKHAT library [20,41,59]. Earlier studies of inclusive jet and dijet production used the POWHEG approach [60]. They exhibit a large dependence on the parton-shower and underlying-event model [21]. We expect that the conclusions drawn from our study will also apply to the simulation provided in [60], as the MC@NLO and POWHEG techniques are of the same formal accuracy.

The outline of this paper is as follows: Section 2 introduces the theoretical framework for our study, including a description of the new developments in SHERPA, which allow to perform the variation of scales in a manner consistent with analytical resummation techniques. Section 3 presents results and discusses the size and relative importance of the various types of uncertainties. Section 4 contains some concluding remarks.

2 The MC@NLO matching method and its uncertainties

This section outlines the essence of the MC@NLO technique for matching next-to-leading order matrix elements and parton showers. We follow the notation introduced in [55] and report on an extension of the MC@NLO implementation therein, which allows to vary resummation scales in a more meaningful way. We point out the free parameters of the MC@NLO method, which will be used to obtain quantitative predictions in Sec. 3.

Notation

In the following, $B(\Phi_B)$ will be used to label Born squared matrix elements, defined on the Born phase space Φ_B, which are summed/averaged over final-/initial-state spins and colours and include parton luminosities as well as symmetry and flux factors. Squared matrix elements of real emission corrections are denoted by $R(\Phi_R)$. They are defined on the real-emission phase space Φ_R. Virtual corrections, including collinear counterterms, are denoted by $\tilde{V}$. Real and virtual corrections induce infrared singularities of opposite sign, which cancel upon integration [61,62]. In order to exploit this cancellation for the construction of Monte-Carlo event generators, subtraction formalisms are invoked [28,29], which introduce real subtraction terms $D_{ij,k}^{(S)}$ and their corresponding integrated counterparts $I_{\widetilde{ij},\tilde{k}}^{(S)}$.

In the MC@NLO method, one defines additional Monte-Carlo counterterms, $D_{ij,k}^{(A)}$, which represent the evolution kernels of the resummation procedure. These counterterms must necessarily have the correct infrared limit in order for the method to maintain full NLO accuracy [55]. Therefore, full colour and spin information needs to be retained. Ordinary parton-shower evolution kernels are recovered from the MC counterterms by taking the limit $N_c \to \infty$ and averaging over spins.

Away from the collinear limit, the form of MC counterterms is less constrained, which essentially presents a source of uncertainty of the MC@NLO method. This particular uncertainty will not be addressed here as it can be reduced by matrix-element parton-shower merging at the next-to-leading order [63–65].

It is particularly useful to identify the MC counterterms with infrared subtraction terms, $D_{ij,k}^{(A)} = D_{ij,k}^{(S)}$, up to phase space constraints. This procedure was advocated in [55], but the corresponding implementation suffered from unknown integrals in the integrated subtraction terms in the case that the phase-space was parametrised in terms of parton-shower evolution and splitting variable. In this publication, the problem is solved by performing the integral of the remainder term $D_{ij,k}^{(A)} - D_{ij,k}^{(S)}$ numerically.

The Mc@Nlo method

In terms of the above defined quantities, omitting flavour- and phase-space mappings, the expectation value of an arbitrary infrared safe observable O in the Mc@Nlo method is given by [52]

$$
\langle O \rangle = \int \mathrm{d}\Phi_B \, \bar{\mathrm{B}}^{(\mathrm{A})}(\Phi_B) \Bigg[\Delta^{(\mathrm{A})}(t_c, \mu_Q^2) \, O(\Phi_B)
$$

$$
+ \sum_{\{\widetilde{\imath\jmath},\tilde{k}\}} \int_{t_c}^{\mu_Q^2} \mathrm{d}\Phi_{R|B}^{ij,k} \, \frac{\mathrm{D}_{ij,k}^{(\mathrm{A})}(\Phi_B, \Phi_{R|B}^{ij,k})}{\mathrm{B}(\Phi_B)} \, \Delta^{(\mathrm{A})}(t, \mu_Q^2) \, O(\Phi_R) \Bigg]
$$

$$
+ \int \mathrm{d}\Phi_R \left[\mathrm{R}(\Phi_R) - \sum_{ij,k} \mathrm{D}_{ij,k}^{(\mathrm{A})}(\Phi_R) \, \Theta(\mu_Q^2 - t) \right] O(\Phi_R) \, .
$$

(2.1)

Therein, Born phase space configurations Φ_B are assigned next-to-leading order weights according to

$$
\bar{\mathrm{B}}^{(\mathrm{A})}(\Phi_B) = \mathrm{B}(\Phi_B) + \tilde{\mathrm{V}}(\Phi_B) + \sum_{\{\widetilde{\imath\jmath},\tilde{k}\}} \mathrm{I}_{\widetilde{\imath\jmath},\tilde{k}}^{(\mathrm{S})}(\Phi_B)
$$

$$
+ \sum_{\{\widetilde{\imath\jmath},\tilde{k}\}} \int \mathrm{d}\Phi_{R|B}^{ij,k} \left[\mathrm{D}_{ij,k}^{(\mathrm{A})}(\Phi_B, \Phi_{R|B}^{ij,k}) \, \Theta(\mu_Q^2 - t) - \mathrm{D}_{ij,k}^{(\mathrm{S})}(\Phi_B, \Phi_{R|B}^{ij,k}) \right] \, .
$$

(2.2)

The real-emission phase space associated with parton emission off an external leg $\widetilde{\imath\jmath}$ of the Born configuration Φ_B can be factorised as $\Phi_R = \Phi_B \cdot \Phi_{R|B}^{ij,k}$. In this context, k denotes spectator partons in the splitting $\widetilde{\imath\jmath}, \tilde{k} \to i, j, k$, which are used to absorb the recoil when a splitting parton $\widetilde{\imath\jmath}$ is put on-shell in the subtraction procedure. The emission phase space, $\mathrm{d}\Phi_{R|B}^{ij,k}$, can be parametrised as $\mathrm{d}\Phi_{R|B}^{ij,k} \propto \mathrm{d}t \, \mathrm{d}z \, \mathrm{d}\phi$, i.e. in terms of an evolution variable t, a splitting variable z and an azimuthal angle ϕ. The evolution variable t is usually identified with some transverse momentum, $\mathrm{k}_\perp^2$. In the above equations, we always assume $t = t(\Phi_{R|B}^{ij,k}) = t(\Phi_R, \Phi_B)$.

We call Eq. (2.2) the next-to-leading order weighted Born cross section. The sum over parton configurations and the integral over the emission phase space in Eq. (2.2) are both evaluated using Monte-Carlo methods, while keeping the Born phase space point, Φ_B, fixed. Because of the choice $\mathrm{D}_{ij,k}^{(\mathrm{A})} = \mathrm{D}_{ij,k}^{(\mathrm{S})}$, the integrand varies only mildly. A single phase-space point is therefore sufficient to obtain a reliable estimate of the integral. Note that in [55] the corresponding integral was absent as the phase-space constraints on $\mathrm{D}_{ij,k}^{(\mathrm{A})}$ were chosen to be the same as on $\mathrm{D}_{ij,k}^{(\mathrm{S})}$. While this method lead to fewer fluctuations of the MC integral, it severely restricted the flexibility of the Mc@Nlo and hampered the correct assessment of uncertainties. In this publication we are able to lift this restriction while still maintaining full next-to-leading order accuracy of the simulation through incorporating full colour and spin information in the resummation.

The resummation procedure itself is encoded in the square bracket multiplying the NLO-weighted Born matrix element, $\bar{\mathrm{B}}^{(\mathrm{A})}$, on the first and second line of Eq. (2.1). Note that the square bracket is unitary by construction. The overall Sudakov factor $\bar{\Delta}^{(\mathrm{A})}$ is defined as

$$
\bar{\Delta}^{(\mathrm{A})}(t, t') = \prod_{\{\widetilde{\imath\jmath},\tilde{k}\}} \bar{\Delta}_{\widetilde{\imath\jmath},\tilde{k}}^{(\mathrm{A})}(t, t') \, ,
$$

(2.3)

with the partial Sudakov factors given by

$$
\bar{\Delta}_{\widetilde{\imath\jmath},\tilde{k}}^{(\mathrm{A})}(t, t') = \exp \left\{ - \sum_{i=q,g} \int_t^{t'} \mathrm{d}\Phi_{R|B}^{ij,k} \, \frac{1}{S_{ij}} \frac{S_R}{S_B} \frac{\mathrm{D}_{ij,k}^{(\mathrm{A})}(\Phi_B, \Phi_{R|B}^{ij,k})}{\mathrm{B}(\Phi_B)} \right\} \, .
$$

(2.4)

Again, $t = t(\Phi_{R|B}^{ij,k})$ is implied and the dependence of the Sudakov factor on the Born phase space configuration is implicit. This Sudakov factor differs from the ordinary parton-shower Sudakov by including full colour and spin correlations. Its implementation is detailed in [55]. The factors S_B, S_R and S_{ij} account for the potentially different symmetry factors present in the Born and real-emission matrix elements and the

3

parton-shower expression, respectively. In the latter, identical particles produced at different scales t are distinguishable, leading to a factorisation of symmetry factors along the evolution chain. The third line in Eq. (2.1) encodes the non-logarithmic remainder terms of the next-to-leading order real-emission correction. Subsequent parton-shower evolution is effected on both terms respecting the emission scales already present. If necessary, truncated parton-shower emission are inserted [53] to retain the logarithmic accuracy of the parton shower.

Uncertainties

The evolution variable in the Monte-Carlo counterterms is limited from above by the resummation scale squared, μ_Q^2. This scale was introduced in the context of analytic resummation [66–70]. It can be used to assess the uncertainties associated with the resummation programme. We will make extensive use of this possibility in Sec. 3.

When defining scales for different parts of the calculation, there are certain restrictions that have to be adhered to. In principle, both the factorisation scale, μ_F, and the renormalisation scale, μ_R, in the NLO weighted Born ME and the hard remainder function can be chosen freely. The difference induced by different scales is formally of $\mathcal{O}(\alpha_s^2)$ relative to the Born contribution. It can, however, have a sizable impact in practice.

A different scale can be chosen for the resummation kernel in the square bracket of Eq. (2.1), which corresponds to the scale employed by the parton shower. This scale is required to be consistent with the one used in the shower itself. In order to achieve full next-to-logarithmic accuracy, it must be of the functional form of the relative transverse momentum of the splitting, $k_\perp$, as $k_\perp \to 0$ [71].

Additional uncertainties arise from subsequent parton showers, hadronization and the simulation of multiple parton scattering. We comment on these effects in the following section.

3 Results

In this section results generated with the MC@NLO algorithm detailed previously are presented for inclusive jet and dijet production. Monte-Carlo predictions are compared to a wide variety of measurements made by both the ATLAS and CMS experiments at the LHC at 7 TeV. The automated implementation of the MC@NLO algorithm in the Monte-Carlo event generator SHERPA, detailed in [55], is used where the only non-automated ingredient, the one-loop matrix element, is interfaced from BLACKHAT [15, 16, 20] employing the methods of [72]. Further QCD evolution is effected using SHERPA's built-in CSS parton shower [73]. Non-perturbative corrections, including multiple parton interactions [74], hadronization corrections [75, 76] and hadron decays [77], are calculated using phenomenological models tuned to data. The standard tune for SHERPA-1.4.0 has been used. Soft-photon corrections are simulated using [78]. The CT10 parton distribution functions [79] have been employed throughout. All results are presented at the particle level, using only stable final state particles with a lifetime longer than 10 ps.

For the central theoretical prediction the scales have been chosen as

$$\mu_F = \mu_R = \tfrac{1}{4}\,H_T \qquad \text{and} \qquad \mu_Q = \tfrac{1}{2}\,p_\perp \;.$$

Therein, H_T is defined as the sum of the scalar transverse momenta of the jets found in the partonic process before applying any resummation. These partonic jets are defined using the anti-$k_\perp$ algorithm [80, 81] with $R = 0.4$ and $p_\perp^{\mathrm{min}} = 20$ GeV. $p_\perp$ is the transverse momentum of any of the two jets of the Born phase space configuration upon which the MC@NLO procedure is effected. To estimate the intrinsic uncertainty of the predictions the perturbative scales μ_F and μ_R have been varied independently by the conventional factor of 2 around the central scale while the resummation scale is kept fixed. For the resummation scale variation, taking into account the simple form of the exponent of the Sudakov factor, the prescription of [67] is followed, varying μ_Q by a factor of $\sqrt{2}$ around the central choice while both μ_F and μ_R are kept fixed. Further, non-perturbative uncertainties, i.e. the impact of shortcomings of the phenomenological models, have been assessed following the prescription outlined in [82]: Alternative tunes increasing and decreasing the mean charged multiplicity in the transverse region by 10% were used to estimate the uncertainty in the multiple parton interaction model[1]. Exchanging the cluster hadronization model of [75, 76] for the Lund

---

[1] This corresponds to changing the switch `SIGMA_ND_FACTOR`∓0.03 (increase/decrease) around the central tune value.
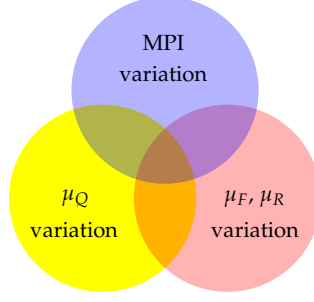
Figure 1: Colour scheme used to display various uncertainties. Overlapping uncertainties will be displayed by adding the colours as indicated.
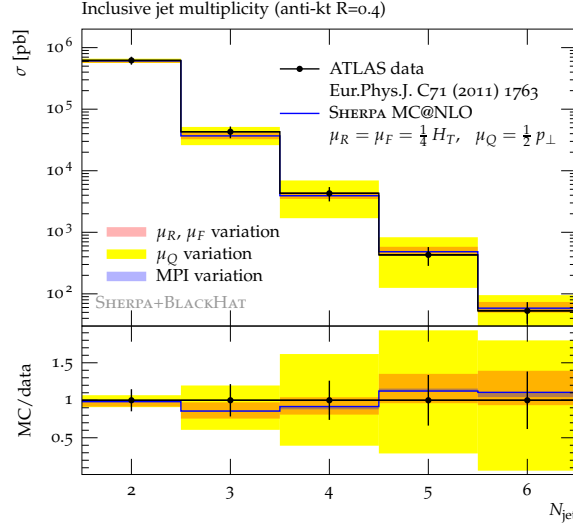
**Figure 2:** Inclusive jet cross section compared to ATLAS data [21].

string hadronization model [83] has been found to have negligible impact on jet observables in previous studies [55, 82], and is therefore not considered here.

All observables studied in the following have been calculated using the same event sample. It is defined by requiring at least two anti-$k_\perp$ jets ($R = 0.4$) with $p_\perp > 10$ GeV at the parton level before applying any resummation, of which at least one must have $p_\perp > 20$ GeV. Fig. 1 presents the colour scheme used to display the individual uncertainties and their overlaps.

Inclusive jet rates

The first observables to study are inclusive jet production rates. These have been measured by the ATLAS collaboration [21]. Jets are defined at the particle level using the anti-$k_\perp$ algorithm with $R = 0.4$ and $p_\perp > 60$ GeV within $|y| < 2.8$. Jets are ordered in transverse momentum. Additionally, the leading jet is required to have $p_\perp > 80$ GeV.

Fig. 2 presents the results. We observe good agreement between our Monte-Carlo simulations and experimental data. The renormalisation and factorisation scale uncertainty amounts to approximately 7% for the dijet inclusive cross-section, which is described at next-to-leading order accuracy, while it increases to 14% for the three-jet inclusive rate, which is described at leading order accuracy only. All higher multiplicity jet inclusive rates are described at the logarithmic accuracy of the parton shower only and therefore inherit the scale uncertainty of the inclusive three-jet rate. The resummation uncertainties, indicating the observables sensitivity to multiple higher-order soft emissions below the resummation scale, is slightly larger: 8% for the dijet inclusive cross section and 35% for the three-jet inclusive rate. They steadily increase for higher jet multiplicities. The non-perturbative uncertainties, on the other hand, are negligible, contributing from ∼0.2% for the dijet cross section to ∼6% for the inclusive 5 jet cross section.
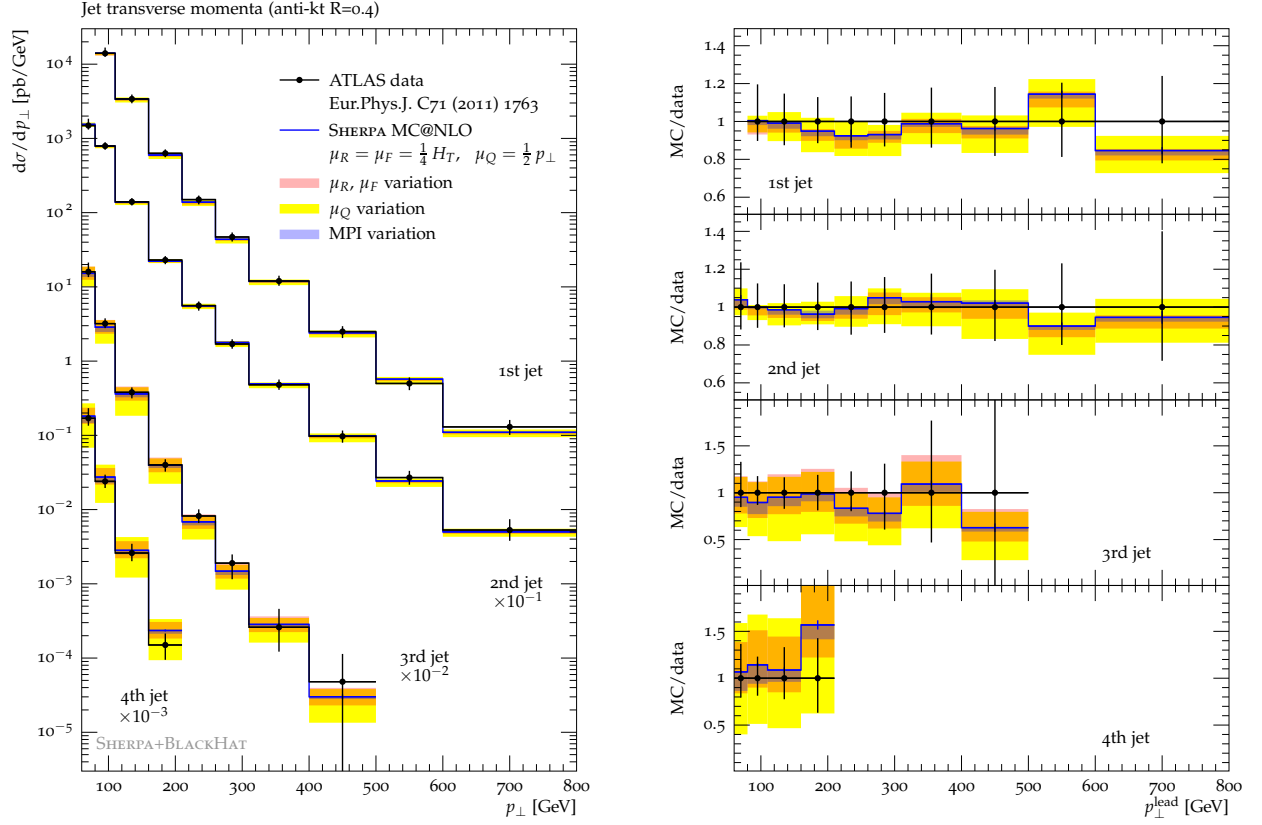
Figure 3: Jet transverse momenta compared to ATLAS data [21].
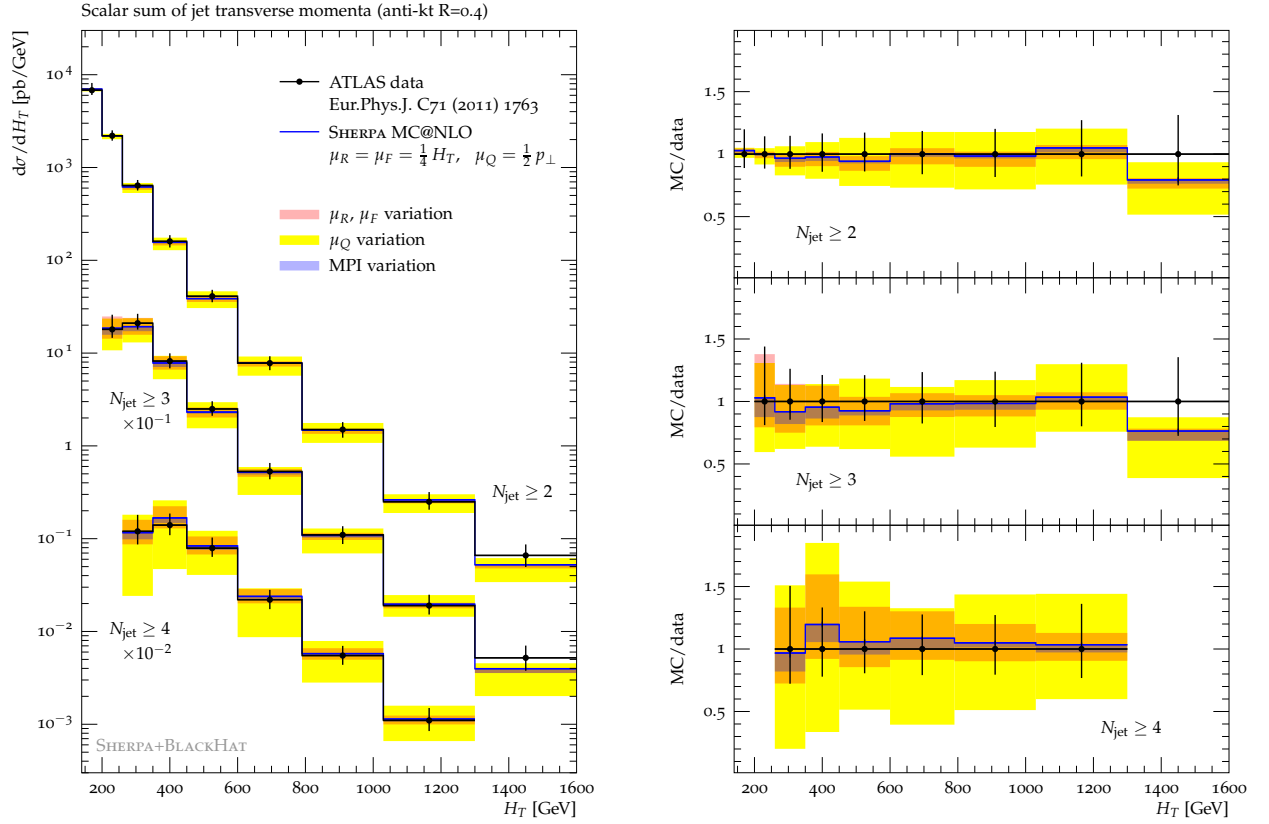
Figure 4: Scalar sum of jet transverse momenta compared to ATLAS data [21].
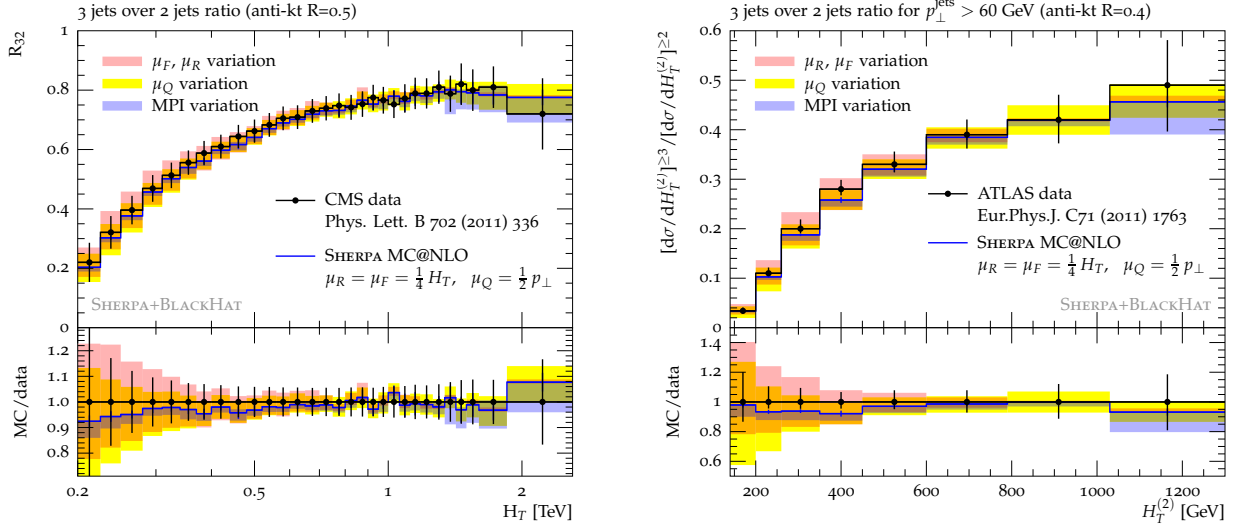
Figure 5: 3-jet over 2-jet ratio in dependence on the scalar transverse momentum sum of all (CMS) and the two leading (ATLAS) jets in comparison to CMS [24] and ATLAS data [21].
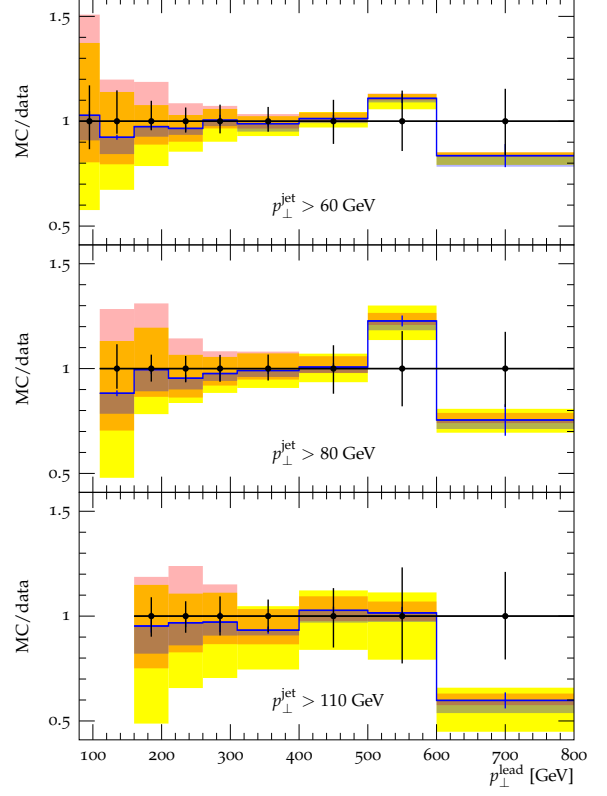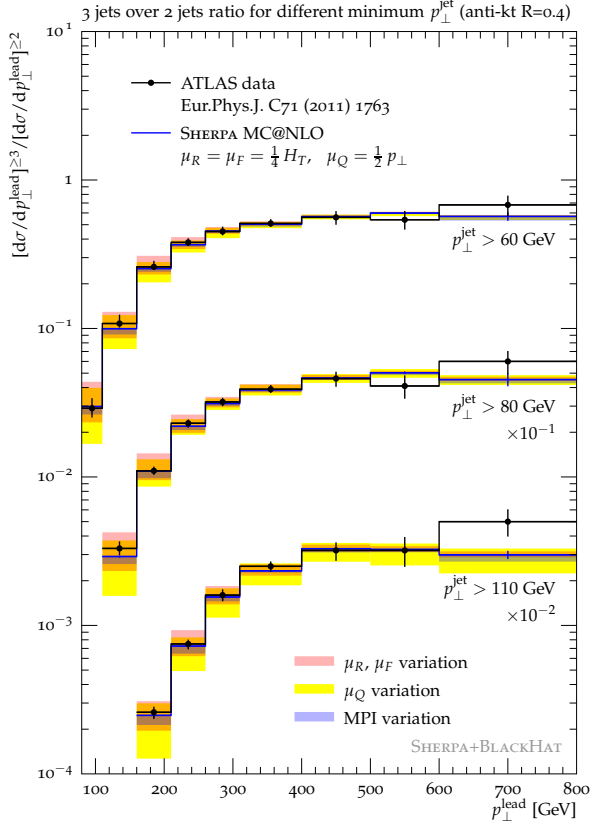
Jet transverse momenta

The same analysis [21] studied also the $p_\perp$-spectra of the individual jets. The event selection is the same as above, except that subleading jets with $p_\perp > 60$ GeV may or may not be present in case of the leading jet $p_\perp$. Fig. 3 displays the results compared to ATLAS data. Again, we observe good agreement with our Monte-Carlo predictions. The two leading jets' transverse momenta, both calculated at next-to-leading order accuracy over large parts of the phase space, show the characteristically small renormalisation and factorisation scale dependencies of $\sim$5-10%. Their resummation scale dependence is comparably very small throughout, ranging from $\sim$5% at low $p_\perp$ to $\sim$20% at large $p_\perp$. This is expected from all choices of the resummation scale being smaller than the second jet's transverse momentum. Any influence therefore stems from the mismatch of (MC@NLO) parton shower evolution and jet reconstruction. The transverse momentum of the third jet, being calculated at leading order accuracy, and the fourth jet, determined at leading logarithmic accuracy only, exhibit much larger scale variation, both for the renormalisation and factorisation scales and the resummation scale. Non-perturbative uncertainties are small in comparison. Similarly, Fig. 4 displays the scalar sum of the individual jet transverse momenta in events with at least two, three or four jets. For these observables good agreement is found as well. The perturbative and non-perturbative uncertainties are comparable to those of the individual jet transverse momenta.

3-jet over 2-jet ratio

The next observable to be examined is the relative rate of inclusive three-jet events compared to inclusive two-jet events. The CMS collaboration measured this ratio in dependence on the scalar sum of all jet transverse momenta, H_T, [24]. Within this analysis events with at least two and three jets, respectively, defined with the anti-$k_\perp$ algorithm with $R = 0.5$, $p_\perp > 50$ GeV, $|y| < 2.5$, and $H_T > 0.2$ TeV were selected. The 3-jet over 2-jet ratio is then defined as $R_{32} = (\mathrm{d}\sigma_{\geq 3\mathrm{jet}}/\mathrm{d}H_T)/(\mathrm{d}\sigma_{\geq 2\mathrm{jet}}/\mathrm{d}H_T)$. The comparison of the presented calculation to data is shown in the left panel of Fig. 5. Good agreement between MC predictions and data is observed. The scale variations in calculating $(\mathrm{d}\sigma_{\geq 3\mathrm{jet}}/\mathrm{d}H_T)$, described at leading order, and $(\mathrm{d}\sigma_{\geq 2\mathrm{jet}}/\mathrm{d}H_T)$, described at next-to-leading order, were done simultaneously because both observables were calculated from the same event sample. Consequently, the renormalisation and factorisation scale uncertainty are large at small H_T but largely cancel at large H_T. The resummation uncertainty behaves similarly, but shows an opposite asymmetry at small H_T. The non-perturbative uncertainties are much smaller for small H_T but grow to equivalent size in the large-H_T region.

The analysis of [21] also studied the 3-jet over 2-jet ratio both as a function of the the scalar transverse momentum sum of the two leading jets, $H_T^{(2)}$, and as a function of the transverse momentum of the leading jet, $p_\perp^{\mathrm{lead}}$, only. The results are displayed in the right panel of Fig. 5 and in Fig. 6, respectively. Both analyses show the same level of agreement between MC predictions and data. Scale uncertainties and non-perturbative uncertainties are of similar size as in the CMS analysis.
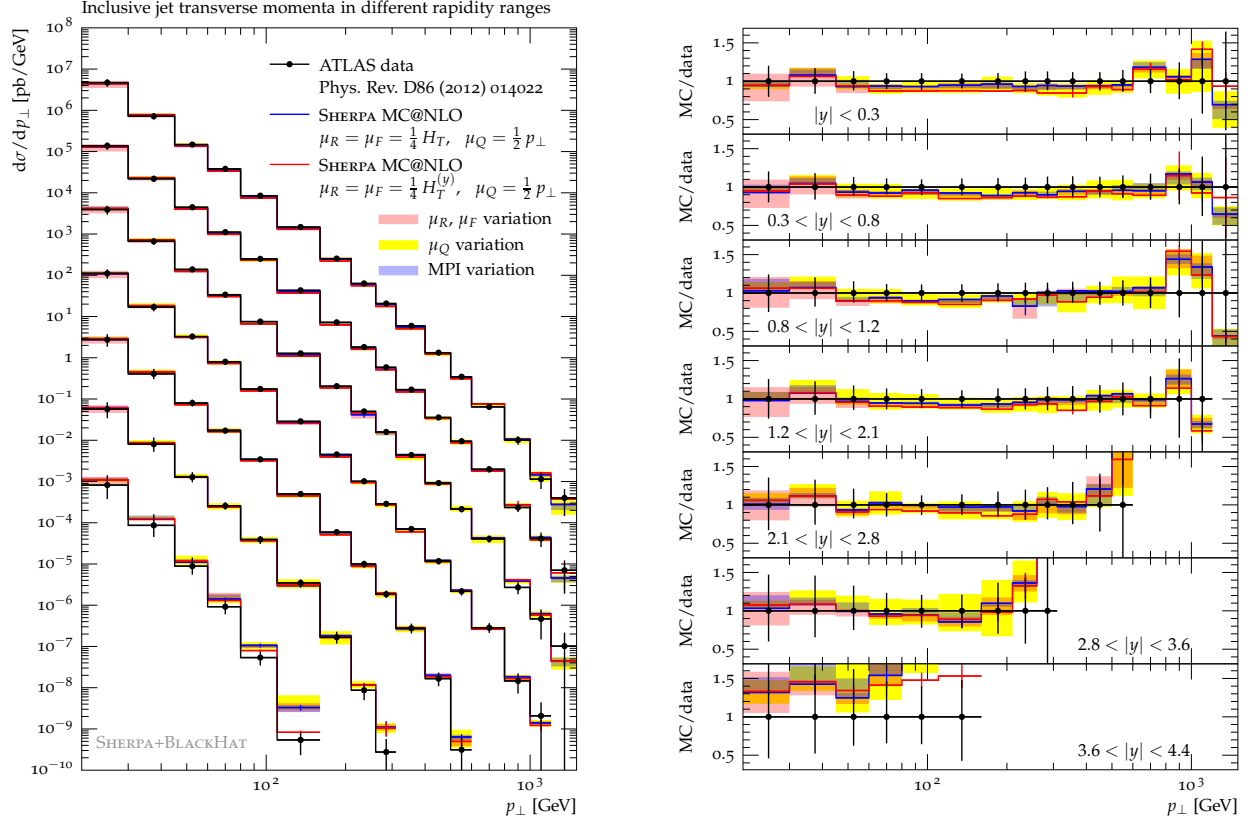
Figure 6: 3-jet over 2-jet ratio in dependence on the leading jet transverse momentum in comparison to ATLAS data [21].
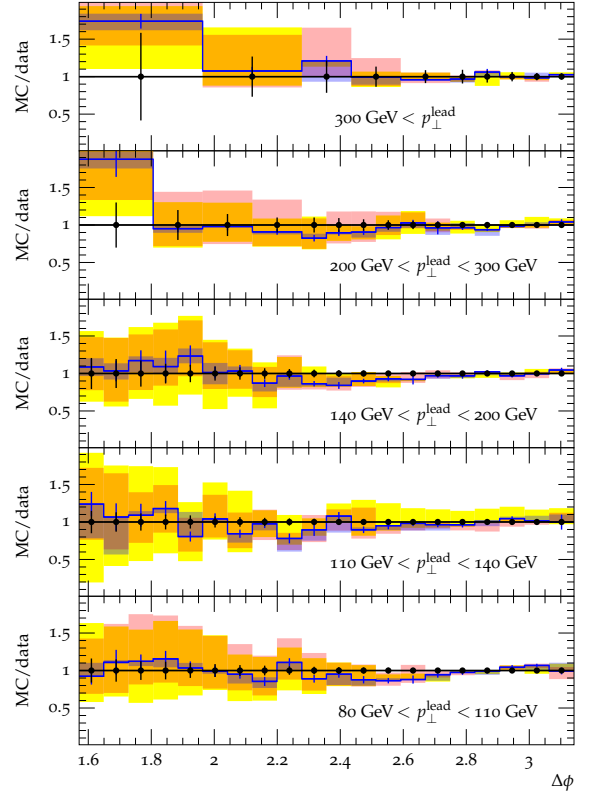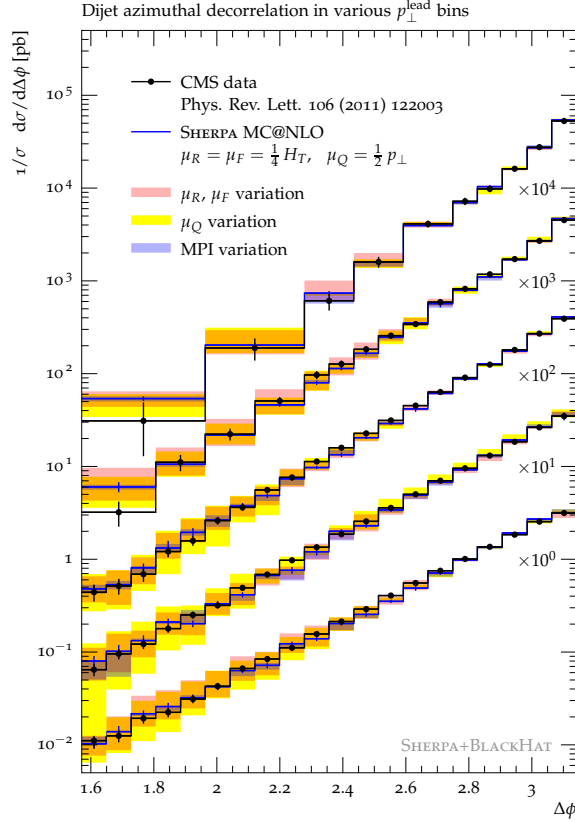
Figure 7: Azimuthal decorrelations of the leading jets compared to CMS data [25]. The individual $p_\perp^{\mathrm{lead}}$ ranges on the left-hand side plot are ordered as indicated in the right-hand side ratio plots.
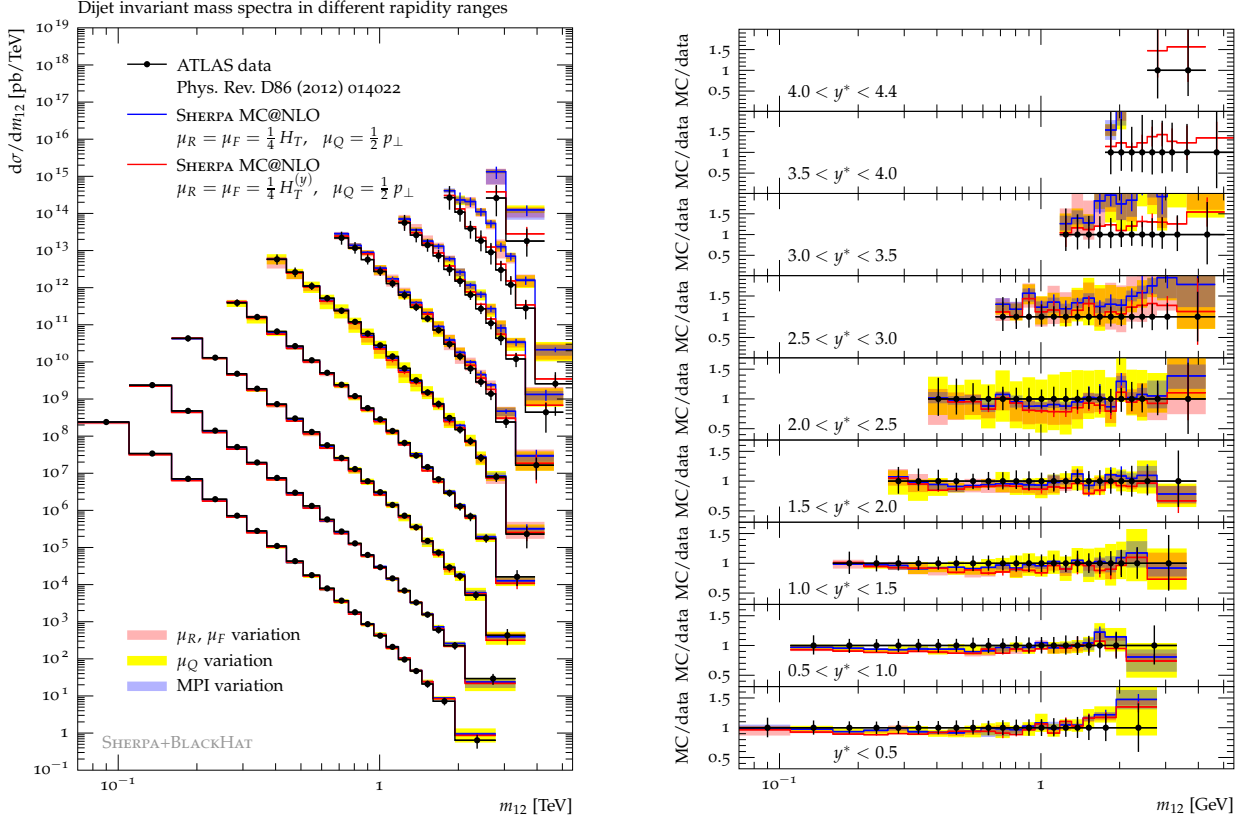
Figure 8: Inclusive jet transverse momenta spectra different rapidity ranges compared to ATLAS data [22]. The different rapidity ranges on the left-hand side plot are ordered as indicated in the right-hand side ratio plots, being multiplied, from top to bottom by factors of 1, $3 \cdot 10^{-2}$, 10^{-3}, $3 \cdot 10^{-5}$, 10^{-6}, $3 \cdot 10^{-8}$, and 10^{-9}, for readabilities sake.

Azimuthal decorrelations

Next, the correlations between the two leading jets are examined. The CMS collaboration measured the dijet azimuthal decorrelations, i.e. the $\Delta\phi$ separation of the two leading jets, in [25]. Therein, the jets are defined using the anti-$k_\perp$ jet algorithm with $R = 0.5$ and a minimum transverse momentum of $p_\perp > 30$ GeV within a rapidity interval of $|y| < 1.1$. Events with at least two such jets were classified according to the leading jet's transverse momentum into five mutually exclusive regions: $p_\perp^{\text{lead}} \in [80, 110]$ GeV, $[110, 140]$ GeV, $[140, 200]$ GeV, $[200, 300]$ GeV, and $[300, \infty)$ GeV. The present calculation provides next-to-leading order accuracy at $\Delta\phi = \pi$, leading order accuracy in the region $\frac{2}{3}\pi < \Delta\phi < \pi$, and leading logarithmic accuracy in the region $\Delta\phi < \frac{2}{3}\pi$. The results are shown in Fig. 7. Good agreement between data and MC prediction is found. The renormalisation and factorisation scale uncertainties are accordingly small in the region $\Delta\phi > \frac{2}{3}\pi$ and increase towards lower $\Delta\phi$ values. Varying the resummation scale leads to similarly large uncertainties, while non-perturbative uncertainties only play a minor role. However, by normalising the observable to the inclusive dijet cross section, the scale uncertainties are artificially reduced.

Inclusive jet transverse momenta in different rapidity ranges

To further study correlations between multiple jets produced, it is useful to consider double-differential observables studied by the ATLAS collaboration [22]. We start with the inclusive jet transverse momentum in different rapidity ranges. Jets are defined using the anti-$k_\perp$ jet algorithm with $R = 0.4$, $p_\perp > 20$ GeV and $|y| < 4.4$. Every jet is considered in the analysis. The contribution from the first two jets in the region where at least two jets are present is described at next-to-leading order accuracy, while the contribution of a possible third jet is described at leading order. All contributions of subsequent jets are described at leading logarithmic accuracy only. Thus, the overall accuracy of these observables is a mixture of the above.

Figure 9: Dijet invariant masses in different rapidity ranges compared to ATLAS data [22]. The rapidity different difference ranges on the left-hand side plot are ordered as indicated in the right-hand side ratio plots, being multiplied, from top to bottom by factors of 10^{12}, $3 \cdot 10^{10}$, 10^9, $3 \cdot 10^8$, 10^6, $3 \cdot 10^4$, 10^3, 30, and 1, for readabilities sake.

Fig. 8 shows the result of the presented calculation compared to data. The agreement in all but the most forward rapidity ranges is good. Renormalisation and factorisation scale uncertainties are small for central jet production while they grow larger with increasing rapidity. The resummation scale uncertainty behaves similarly albeit being larger in magnitude throughout. Non-perturbative uncertainties are small, except in the very forward region, close to the beams. At very large rapidities the transverse momentum is no longer a good measure of the hardness of the process [13, 14, 84]. Instead a scale taking into account the dijet invariant mass should be used. Such consideration applied to an H_T-based scale, taking into account real emission dynamics, is proposed to take the following form

$$\mu_{R/F} \;=\; \tfrac{1}{4}\, H_T^{(y)} \;=\; \tfrac{1}{4} \cdot \sum_{i \in \mathrm{jets}} |p_{\perp,i}|\, e^{f\,|y - y_{\mathrm{boost}}|} \tag{3.1}$$

wherein $y_{\mathrm{boost}} = 1/n_{\mathrm{jet}} \cdot \sum_{i \in \mathrm{jets}} y_i$, the rapidity of the n-jet system. The factor f is chosen to suitably interpolate between the invariant-mass-like behaviour and transverse-momentum-like behaviour. For $f = 0.3$ and the presence of only two jets it reduces exactly to the scale proposed in [13,14,84], $\mu_{R/F} = \tfrac{1}{2}\, p_\perp\, e^{0.3 y^*} \approx m_{12}/(4\cosh(0.7 y^*))$. This scale choice, however, is only beneficial for describing data in this and the following analysis and either shows no impact or even reduces the agreement with the observed experimental data in all other analyses considered in this publication[2]. It is therefore not adopted as a central scale choice.

Dijet invariant masses in different rapidity ranges

Another doubly differential observable studied in [22] is the dijet invariant mass. Events with at least two anti-$k_\perp$ jets with $R = 0.4$ and $p_\perp^{\mathrm{lead}} > 30$ GeV and $p_\perp^{\mathrm{sublead}} > 20$ GeV within $|y| < 4.4$ are considered.

---

[2] Taking $\mu_{R/F} = \tfrac{1}{4}\, H_T^{(y)}$ as the central scale leads to an underestimation of the inclusive three-jet rate presented in Fig. 2 by 30%, for example.

The dijet invariant mass is defined $m_{12} = \sqrt{(p^{\text{lead}} + p^{\text{sublead}})^2}$ and binned into various mutually exclusive ranges of $y^* = \frac{1}{2}|y_{\text{lead}} - y_{\text{sublead}}|$, the rapidity separation of the two jets. Fig. 9 displays MC results compared to ATLAS data. For small rapidity separations the agreement with data is good. At large y^* the renormalisation and factorisation scale is too low, resulting in too large MC predictions. This situation is improved by choosing the scale Eq. (3.1) instead. The renormalisation and resummation scale uncertainties are small at small y^* and increase towards larger y^*. They also remain approximately constant over the whole considered m_{12} range. Resummation scale uncertainties, on the other hand, are larger and display a definite m_{12} dependence. This can be seen as an indication that high-energy resummation, which goes beyond the collinear limit used in the parton shower, becomes important [85–87]. Non-perturbative uncertainties are only non-negligible at low invariant masses or large rapidity separations, when at least one jet is likely to be close to either of the two beams.

As discussed in the previous paragraph, taking $\frac{1}{4}H_T^{(y)}$ as the central scale improves the description of this observable but leads to a worse description of the other observables investigated in this paper. It is therefore not adopted as the central scale.

Gap fractions

A different way to probe the radiation pattern was explored by the ATLAS collaboration in [23]. Therein, events were selected containing at least two jets, defined using the anti-$k_\perp$ algorithm with $R = 0.6$, each with $p_\perp > 20$ GeV within $y < 4.4$. Within these events a dijet system is then identified using either the two largest transverse momentum jets (leading jet selection) or the widest separated jets (forward backward selection). For both definitions an average transverse momentum $\bar{p}_\perp = \frac{1}{2}(p_\perp^{\text{jet1}} + p_\perp^{\text{jet2}})$ of at least 50 GeV is required. To characterise the subsequent radiation pattern two variables are used. The gap fraction, i.e. the fraction of events that do not exhibit any further radiation above some Q_0 within the Δy rapidity range spanned by the dijet system, and the mean number of jets with $p_\perp > Q_0$ in the same Δy region. Fig. 10 displays a comparison of MC results with data for the gap fraction ($Q_0 = 20$ GeV) in dependence on the rapidity separation of the dijet system and its $\bar{p}_\perp$ for both selections. The agreement is good throughout the probed region. In both selections the renormalisation and factorisation scale uncertainty is the leading uncertainty at low $\bar{p}_\perp$ while the resummation uncertainty dominates at large $\bar{p}_\perp$. Non-perturbative uncertainties are generally larger than for most other observables considered in this paper, increasing with Δy and $\bar{p}_\perp$. In case of the forward backward selection they are of the same magnitude as both perturbative uncertainties in the large Δy and $\bar{p}_\perp$ region.

Similarly, Fig. 11 displays the average number of jets ($Q_0 = 20$ GeV) in dependence on the rapidity separation of the dijet system and its $\bar{p}_\perp$ for both selections. Again, good agreement is found. All uncertainties are small and of comparable size for small Δy throughout the $\bar{p}_\perp$ range, and steadily increasing for larger Δy. While a resummation scale variation produces largely $\bar{p}_\perp$ independent uncertainties the renormalisation and factorisation scale uncertainties are larger for small average transverse momenta than for large ones. The non-perturbative uncertainties show the opposite behaviour.

Event shapes

Traditional observables not being described without resummation are event shapes. The CMS collaboration measured the central transverse thrust and the central transverse thrust minor in multijet production in [26]. The sample is defined by requiring at least two jets, defined using the anti-$k_\perp$ algorithm with $R = 0.5$, $p_\perp > 30$ GeV and $|\eta| < 1.3$. The selected events are then categorised into three mutually exclusive regions according to the leading jet transverse momentum. The observables are defined as follows

$$\tau_{\perp,C} = 1 - \max_{\hat{n}_T} \frac{\sum_{i\in\text{jets}} |\vec{p}_{\perp,i} \cdot \hat{n}_T|}{\sum_{i\in\text{jets}} |\vec{p}_{\perp,i}|} \qquad \text{and} \qquad T_{m,C} = \frac{\sum_{i\in\text{jets}} |\vec{p}_{\perp,i} \times \hat{n}_{T,C}|}{\sum_{i\in\text{jets}} |\vec{p}_{\perp,i}|} \; .$$

Therein, the vector $n_{T,C}$ is defined as the vector minimising $\tau_{\perp,C}$. Only jet momenta are taken into account. The results of the presented calculation are compared to the experimental data in Fig. 12. Good agreement between MC predictions and data is found. The dependence of both observables on the renormalisation and factorisation scale, despite being calculated at most at leading order accuracy, largely cancels due to their normalisation. However, they do show a large dependence on the resummation scale, as expected. This
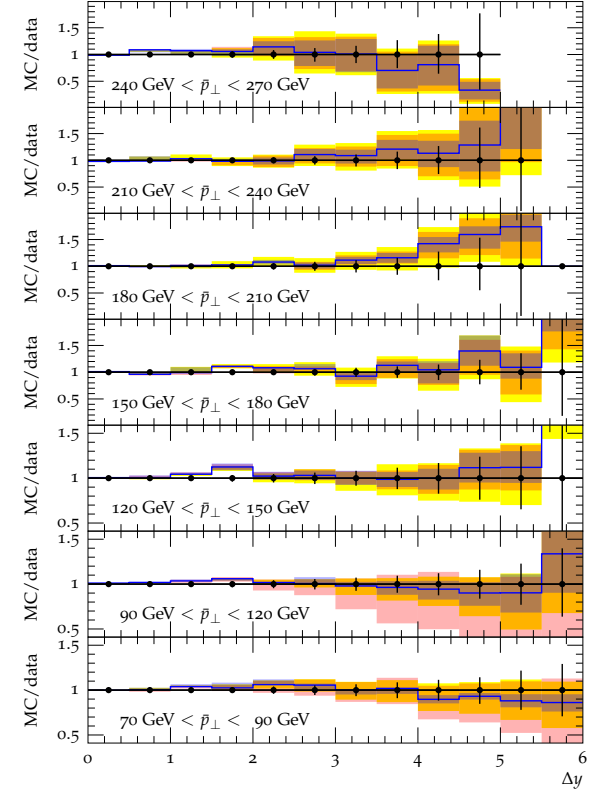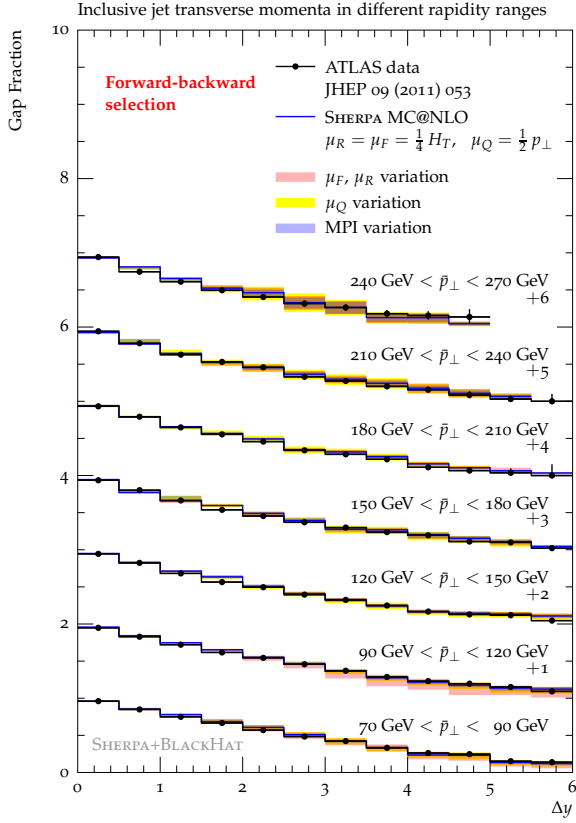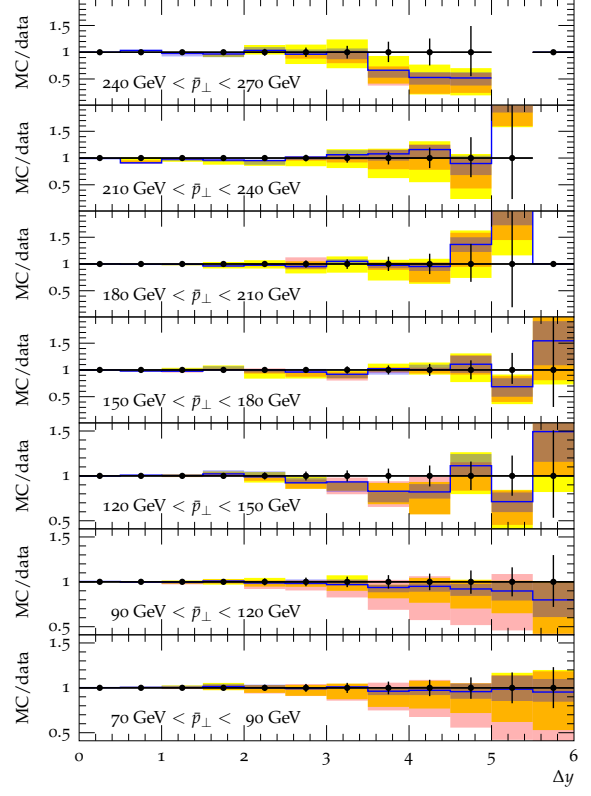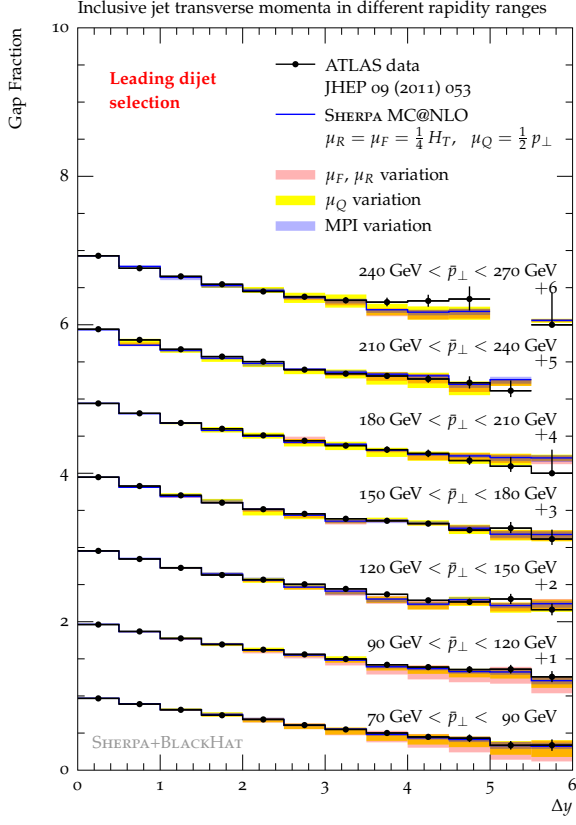
Figure 10: Gap fraction in dependence of mean transverse momentum and rapidity separation of dijet pair for both selections compared to ATLAS data [23].
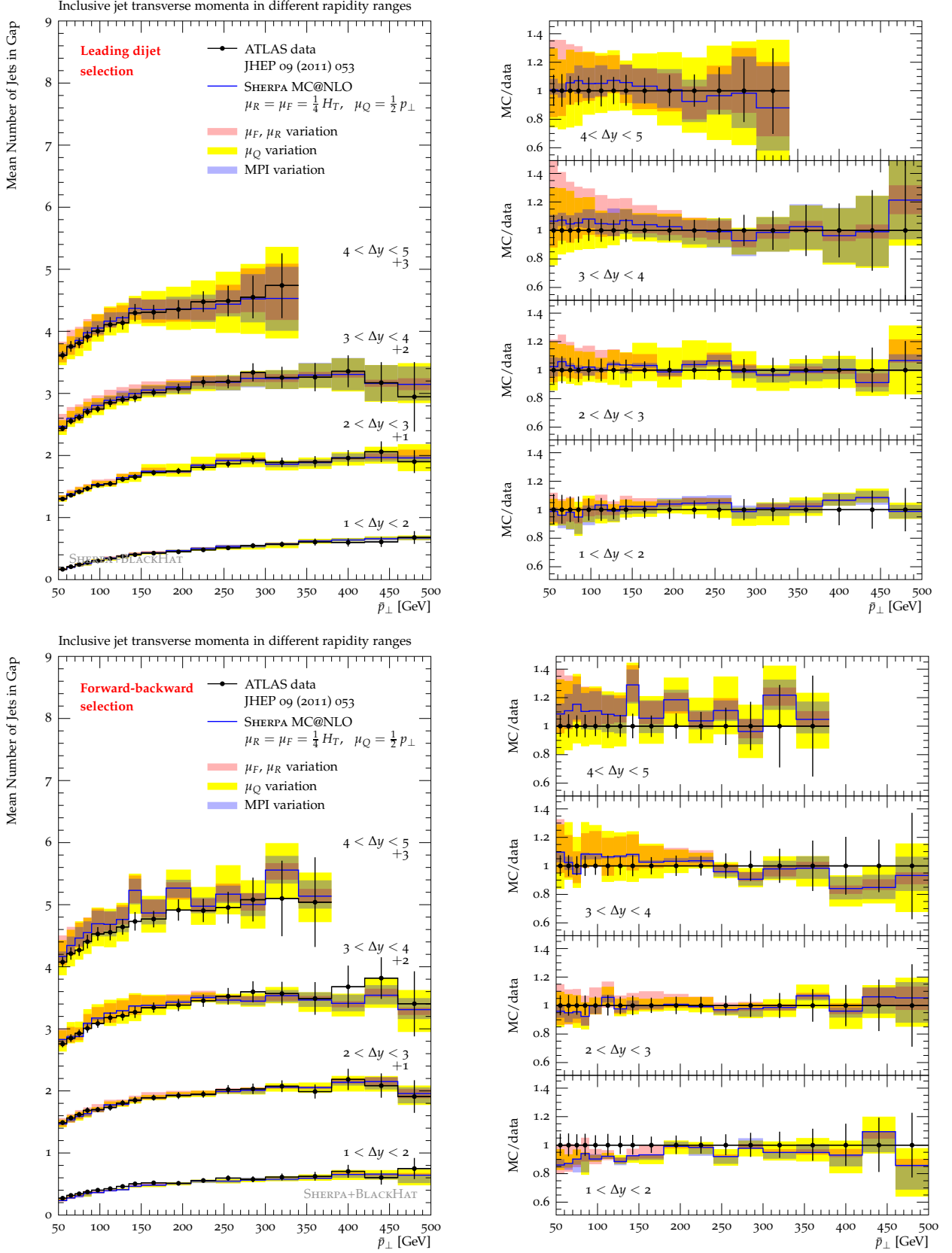
Figure 11: Mean jet number in gap in dependence of mean transverse momentum and rapidity separation of dijet pair for both selections compared to ATLAS data [23].
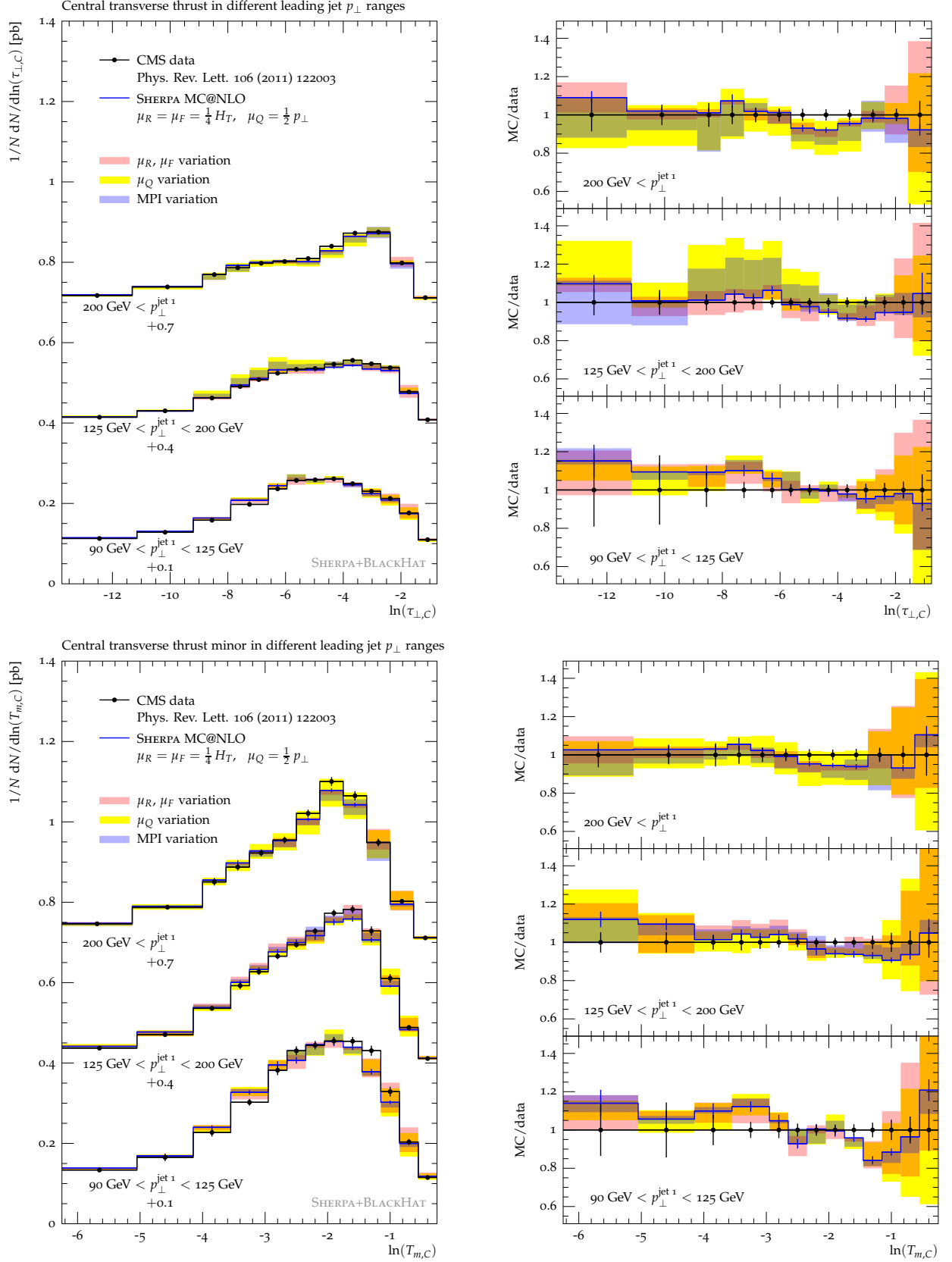
Figure 12: Central transverse thrust and central transverse thrust minor compared to CMS data [26].

14
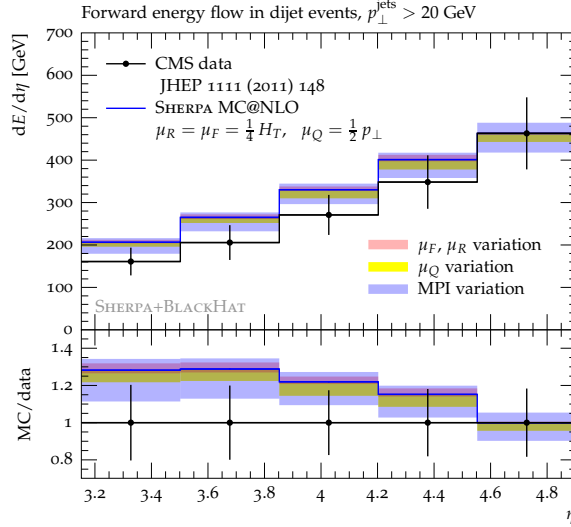
Figure 13: Forward energy flow compared to CMS data [27].

is largest when $\tau_{\perp,C}$ ($T_{m,C}$) is close to zero (one). The non-perturbative uncertainties have the opposite behaviour.

Forward energy flow

The last observable to be studied is the forward energy flow as measured by the CMS collaboration [27]. In this analysis, events with at least two jets, defined by the anti-$k_\perp$ algorithm with $R = 0.5$ and $p_\perp > 20$ GeV are required. The two leading jets are further required to lie within $|\eta| < 2.5$ and satisfy $|\Delta\phi - \pi| < 1$, i.e. to produce a nearly back-to-back topology. Within this event sample the energy flow, defined as average energy E per event per pseudo-rapidity interval $\mathrm{d}\eta$, is calculated and compared to the measured data. Despite a small difference in shape good agreement is found. Again, due to the normalisation of the observable, renormalisation and factorisation scale uncertainties as well as resummation scale uncertainties are small. A comparably large uncertainty stems from the non-perturbative modelling uncertainties, ranging up to $\sim 10\%$. This is not unexpected since in this very forward region, close to the beams, non-factorizable components of the inclusive cross section play a large role.

4   Conclusions

We have presented a detailed analysis of uncertainties associated with the simulation of inclusive jet and dijet production using methods for matching next-to-leading order QCD calculations and parton showers. We have analysed factorisation and renormalisation scale dependence as well as variations originating from the choice of resummation scale. We have compared to uncertainties originating from the freedom in choosing parameters in the Monte-Carlo simulation of multiple parton scattering.

These three types of uncertainties represent different degrees of freedom in the Monte-Carlo simulation: While the renormalisation and factorisation scale dependence probe the impact of higher-order QCD corrections to the hard process, the resummation scale dependence quantifies, to some extent, uncertainties related to parton evolution. Variations of the MPI tune are used to estimate uncertainties related to non-perturbative dynamics.

The results of our Monte-Carlo simulation have been compared to a variety of data taken by the ATLAS and CMS experiments at the CERN LHC. Good agreement is found for almost all observables. Exceptions are the inclusive jet transverse momenta at large jet rapidity and the dijet invariant masses at large average rapidity. Discrepancies are attributed to the choice of renormalisation and factorisation scale, which is given by one quarter of the visible transverse energy. Despite taking into account real-emission dynamics, this scale does not give a realistic measure of the hardness of events at large individual jet rapidities. A modified scale, with jet transverse momenta weighted by their rapidity w.r.t. the centre of the partonic system, leads

to better agreement in the forward region, but deviations are observed for central jet production.

Uncertainties related to higher-order corrections to the hard process are most important for exclusive multi-jet final states. Similarly, uncertainties related to the resummation procedure are most significant in the region where jet production is modelled by the parton shower. We expect that both uncertainties can be reduced by application of matrix-element parton-shower merging methods at the next-to-leading order [63–65]. A corresponding analysis is forthcoming. A different role is played by non-perturbative uncertainties. They are most significant in regions where (semi-)soft particle production dominates over multi-jet effects. They can be reduced only by better constraints on the non-perturbative dynamics through additional measurements of underlying event activity and particle flow.

Our analysis should help to better understand the quality of Monte-Carlo predictions, which are obtained using matching methods like McNLO and Powheg. Ascribing reliable uncertainties to such predictions will remain an important task in the immediate future of LHC physics.

Acknowledgements

References

[1] R. S. Chivukula, M. Golden and E. H. Simmons, *Multi - jet physics at hadron colliders*, Nucl.Phys. **B363** (1991), 83–96.

[2] L. J. Dixon and Y. Shadmi, *Testing gluon selfinteractions in three jet events at hadron colliders*, Nucl.Phys. **B423** (1994), 3–32, [`arXiv:hep-ph/9312363 [hep-ph]`].

[3] C. Kilic, S. Schumann and M. Son, *Searching for Multijet Resonances at the LHC*, JHEP **04** (2009), 128, [`arXiv:0810.5542 [hep-ph]`].

[4] T. Han, I. Lewis and Z. Liu, *Colored Resonant Signals at the LHC: Largest Rate and Simplest Topology*, JHEP **1012** (2010), 085, [`arXiv:1010.4309 [hep-ph]`].

[5] Y. Bai and J. Shelton, *Composite Octet Searches with Jet Substructure*, JHEP **1207** (2012), 067, [`arXiv:1107.3563 [hep-ph]`].

[6] S. Schumann, A. Renaud and D. Zerwas, *Hadronically decaying color-adjoint scalars at the LHC*, JHEP **1109** (2011), 074, [`arXiv:1108.2957 [hep-ph]`].

[7] M. Guzzi, P. Nadolsky, E. Berger, H.-L. Lai, F. Olness et al., *CT10 parton distributions and other developments in the global QCD analysis*, `arXiv:1101.0561 [hep-ph]`.

[8] A. D. Martin, W. J. Stirling, R. S. Thorne and G. Watt, *Parton distributions for the LHC*, Eur. Phys. J. **C63** (2009), 189–295, [`arXiv:0901.0002 [hep-ph]`].

[9] R. D. Ball, V. Bertone, S. Carrazza, C. S. Deans, L. Del Debbio et al., *Parton distributions with LHC data*, `arXiv:1207.1303 [hep-ph]`.

[10] T. Affolder et al., CDF Collaboration collaboration, *Measurement of the strong coupling constant from inclusive jet production at the Tevatron $p\bar{p}$ collider*, Phys.Rev.Lett. **88** (2002), 042001, [`arXiv:hep-ex/0108034 [hep-ex]`].

[11] V. Abazov et al., D0 Collaboration collaboration, *Determination of the strong coupling constant from the inclusive jet cross section in $p\bar{p}$ collisions at sqrt(s)=1.96 TeV*, Phys.Rev. **D80** (2009), 111107, [`arXiv:0911.2710 [hep-ex]`].

[12] M. Wobisch, D0 Collaboration collaboration, *Determination of the Strong Coupling Constant and Multijet Cross Section Ratio Measurements*, `arXiv:1106.5132` [hep-ex].

[13] S. D. Ellis, Z. Kunszt and D. E. Soper, *The one jet inclusive cross-section at order α_s^3 quarks and gluons*, Phys.Rev.Lett. **64** (1990), 2121.

[14] S. D. Ellis, Z. Kunszt and D. E. Soper, *Two jet production in hadron collisions at order α_s^3 in QCD*, Phys.Rev.Lett. **69** (1992), 1496–1499.

[15] W. Giele, E. N. Glover and D. A. Kosower, *Higher order corrections to jet cross-sections in hadron colliders*, Nucl.Phys. **B403** (1993), 633–670, [`arXiv:hep-ph/9302225` [hep-ph]].

[16] W. Giele, E. N. Glover and D. A. Kosower, *The Two-Jet Differential Cross Section at $\mathcal{O}(\alpha_s^3)$ in Hadron Collisions*, Phys.Rev.Lett. **73** (1994), 2019–2022, [`arXiv:hep-ph/9403347` [hep-ph]].

[17] W. B. Kilgore and W. Giele, *Next-to-leading order gluonic three jet production at hadron colliders*, Phys.Rev. **D55** (1997), 7183–7190, [`arXiv:hep-ph/9610433` [hep-ph]].

[18] Z. Nagy, *Three jet cross-sections in hadron hadron collisions at next-to-leading order*, Phys.Rev.Lett. **88** (2002), 122003, [`arXiv:hep-ph/0110315` [hep-ph]].

[19] Z. Nagy, *Next-to-leading order calculation of three-jet observables in hadron-hadron collisions*, Phys. Rev. **D68** (2003), 094002, [`hep-ph/0307268`].

[20] Z. Bern, G. Diana, L. Dixon, F. Febres Cordero, S. Hoeche et al., *Four-Jet Production at the Large Hadron Collider at Next-to-Leading Order in QCD*, `arXiv:1112.3940` [hep-ph].

[21] G. Aad et al., ATLAS Collaboration collaboration, *Measurement of multi-jet cross sections in proton-proton collisions at a 7 TeV center-of-mass energy*, Eur.Phys.J. **C71** (2011), 1763, [`arXiv:1107.2092` [hep-ex]].

[22] G. Aad et al., ATLAS Collaboration collaboration, *Measurement of inclusive jet and dijet production in pp collisions at sqrt(s) = 7 TeV using the ATLAS detector*, Phys. Rev. **D86** (2012), 014022, [`arXiv:1112.6297` [hep-ex]].

[23] G. Aad et al., ATLAS collaboration, *Measurement of dijet production with a veto on additional central jet activity in pp collisions at $\sqrt{s}=7$ TeV using the ATLAS detector*, `arXiv:1107.1641` [hep-ex].

[24] S. Chatrchyan et al., CMS Collaboration collaboration, *Measurement of the Ratio of the 3-jet to 2-jet Cross Sections in pp Collisions at $\sqrt{s} = 7$ TeV*, Phys.Lett. **B702** (2011), 336–354, [`arXiv:1106.0647` [hep-ex]].

[25] V. Khachatryan et al., CMS Collaboration collaboration, *Dijet Azimuthal Decorrelations in pp Collisions at $\sqrt{s} = 7$ TeV*, Phys.Rev.Lett. **106** (2011), 122003, [`arXiv:1101.5029` [hep-ex]].

[26] V. Khachatryan et al., CMS collaboration, *First Measurement of Hadronic Event Shapes in pp Collisions at $\sqrt{s}=7$ TeV*, Phys. Lett. **B699** (2011), 48–67, [`arXiv:1102.0068` [hep-ex]].

[27] S. Chatrchyan et al., CMS Collaboration collaboration, *Measurement of energy flow at large pseudorapidities in pp collisions at $\sqrt{s} = 0.9$ and 7 TeV*, JHEP **1111** (2011), 148, [`arXiv:1110.0211` [hep-ex]].

[28] S. Frixione, Z. Kunszt and A. Signer, *Three-jet cross-sections to next-to-leading order*, Nucl. Phys. **B467** (1996), 399–442, [`hep-ph/9512328`].

[29] S. Catani and M. H. Seymour, *A general algorithm for calculating jet cross sections in NLO QCD*, Nucl. Phys. **B485** (1997), 291–419, [`hep-ph/9605323`].

[30] S. Catani, S. Dittmaier, M. H. Seymour and Z. Trocsanyi, *The dipole formalism for next-to-leading order QCD calculations with massive partons*, Nucl. Phys. **B627** (2002), 189–265, [`hep-ph/0201036`].

[31] T. Gleisberg and F. Krauss, *Automating dipole subtraction for QCD NLO calculations*, Eur. Phys. J. **C53** (2008), 501–523, [`arXiv:0709.2881` [hep-ph]].

[32] R. Frederix, T. Gehrmann and N. Greiner, *Automation of the Dipole Subtraction Method in Mad-Graph/MadEvent*, JHEP **09** (2008), 122, [`arXiv:0808.2128` [hep-ph]].

[33] M. Czakon, C. Papadopoulos and M. Worek, *Polarizing the dipoles*, JHEP **08** (2009), 085, [`arXiv:0905.0883` [hep-ph]].

[34] R. Frederix, S. Frixione, F. Maltoni and T. Stelzer, *Automation of next-to-leading order computations in QCD: the FKS subtraction*, JHEP **10** (2009), 003, [`arXiv:0908.4272` [hep-ph]].

[35] R. Frederix, T. Gehrmann and N. Greiner, *Integrated dipoles with MadDipole in the MadGraph framework*, JHEP **06** (2010), 086, [`arXiv:1004.2905` [hep-ph]].

[36] A. Denner and S. Dittmaier, *Reduction schemes for one-loop tensor integrals*, Nucl. Phys. **B734** (2006), 62–115, [`arXiv:hep-ph/0509141` [hep-ph]].

[37] G. Ossola, C. G. Papadopoulos and R. Pittau, *Reducing full one-loop amplitudes to scalar integrals at the integrand level*, Nucl. Phys. **B763** (2007), 147–169, [`hep-ph/0609007`].

[38] R. Ellis, W. Giele and Z. Kunszt, *A numerical unitarity formalism for evaluating one-loop amplitudes*, JHEP **0803** (2008), 003, [`arXiv:0708.2398` [hep-ph]].

[39] T. Binoth, J. P. Guillet, G. Heinrich, E. Pilon and T. Reiter, *Golem95: A numerical program to calculate one-loop tensor integrals with up to six external legs*, Comput. Phys. Commun. **180** (2009), 2317–2330, [`arXiv:0810.0992` [hep-ph]].

[40] G. Ossola, C. G. Papadopoulos and R. Pittau, *On the rational terms of the one-loop amplitudes*, JHEP **05** (2008), 004, [`arXiv:0802.1876` [hep-ph]].

[41] C. F. Berger, Z. Bern, L. J. Dixon, F. Febres-Cordero, D. Forde, H. Ita, D. A. Kosower and D. Maître, *Automated implementation of on-shell methods for one-loop amplitudes*, Phys. Rev. **D78** (2008), 036003, [`arXiv:0803.4180` [hep-ph]].

[42] R. Ellis, W. T. Giele, Z. Kunszt and K. Melnikov, *Masses, fermions and generalized D-dimensional unitarity*, Nucl. Phys. **B822** (2009), 270–282, [`arXiv:0806.3467` [hep-ph]].

[43] R. Ellis, K. Melnikov and G. Zanderighi, *W + 3 jet production at the Tevatron*, Phys. Rev. **D80** (2009), 094002, [`arXiv:0906.1445` [hep-ph]].

[44] C. F. Berger, Z. Bern, L. J. Dixon, F. Febres-Cordero, D. Forde, T. Gleisberg, H. Ita, D. A. Kosower and D. Maître, *Precise Predictions for W + 4-Jet Production at the Large Hadron Collider*, Phys. Rev. Lett. **106** (2011), 092001, [`arXiv:1009.2338` [hep-ph]].

[45] H. Ita, Z. Bern, L. J. Dixon, F. Febres-Cordero, D. A. Kosower and D. Maître, *Precise Predictions for Z + 4 Jets at Hadron Colliders*, Phys.Rev. **D85** (2012), 031501, [`arXiv:1108.2229` [hep-ph]].

[46] A. Denner, S. Dittmaier, S. Kallweit and S. Pozzorini, *NLO QCD corrections to WWbb production at hadron colliders*, Phys. Rev. Lett. **106** (2011), 052001, [`1012.3975` [hep-ph]].

[47] A. Bredenstein, A. Denner, S. Dittmaier and S. Pozzorini, *NLO QCD corrections to top anti-top bottom anti-bottom production at the LHC: 2. full hadronic results*, JHEP **1003** (2010), 021, [`arXiv:1001.4006` [hep-ph]].

[48] G. Cullen et al., *Automated One-Loop Calculations with GoSam*, `arXiv:1111.2034` [hep-ph].

[49] G. Cullen, N. Greiner, G. Heinrich, G. Luisoni, P. Mastrolia et al., *GoSam: A program for automated one-loop Calculations*, `arXiv:1111.6534` [hep-ph].

[50] F. Cascioli, P. Maierhofer and S. Pozzorini, *Scattering Amplitudes with Open Loops*, `arXiv:1111.5206` [hep-ph].

[51] V. Hirschi, R. Frederix, S. Frixione, M. V. Garzelli, F. Maltoni and R. Pittau, *Automation of one-loop QCD corrections*, JHEP **1105** (2011), 044, [`arXiv:1103.0621` [hep-ph]].

[52] S. Frixione and B. R. Webber, *Matching NLO QCD computations and parton shower simulations*, JHEP **06** (2002), 029, [`hep-ph/0204244`].

[53] P. Nason, *A new method for combining NLO QCD with shower Monte Carlo algorithms*, JHEP **11** (2004), 040, [`hep-ph/0409146`].

[54] S. Frixione, P. Nason and C. Oleari, *Matching NLO QCD computations with parton shower simulations: the POWHEG method*, JHEP **11** (2007), 070, [`arXiv:0709.2092` [hep-ph]].

[55] S. Höche, F. Krauss, M. Schönherr and F. Siegert, *A critical appraisal of NLO+PS matching methods*, `arXiv:1111.1220` [hep-ph].

[56] P. Nason and B. Webber, *Next-to-Leading-Order Event Generators*, `arXiv:1202.1251` [hep-ph].

[57] T. Gleisberg, S. Höche, F. Krauss, A. Schälicke, S. Schumann and J. Winter, *SHERPA 1.α, a proof-of-concept version*, JHEP **02** (2004), 056, [`hep-ph/0311263`].

[58] T. Gleisberg, S. Höche, F. Krauss, M. Schönherr, S. Schumann, F. Siegert and J. Winter, *Event generation with SHERPA 1.1*, JHEP **02** (2009), 007, [`arXiv:0811.4622` [hep-ph]].

[59] C. F. Berger, Z. Bern, L. J. Dixon, F. Febres-Cordero, D. Forde, T. Gleisberg, H. Ita, D. A. Kosower and D. Maître, *Precise Predictions for W + 3 Jet Production at Hadron Colliders*, Phys. Rev. Lett. **102** (2009), 222001, [`arXiv:0902.2760` [hep-ph]].

[60] S. Alioli, K. Hamilton, P. Nason, C. Oleari and E. Re, *Jet pair production in POWHEG*, JHEP **1104** (2011), 081, [`arXiv:1012.3380` [hep-ph]].

[61] T. Kinoshita, *Mass Singularities of Feynman Amplitudes*, J.Math.Phys. **3** (1962), 650–677.

[62] T. Lee and M. Nauenberg, *Degenerate Systems and Mass Singularities*, Phys. Rev. **133** (1964), B1549–B1562.

[63] N. Lavesson and L. Lönnblad, *Extending CKKW-merging to one-loop matrix elements*, JHEP **12** (2008), 070, [`arXiv:0811.2912` [hep-ph]].

[64] T. Gehrmann, S. Höche, F. Krauss, M. Schönherr and F. Siegert, *NLO QCD matrix elements + parton showers in $e^+e^- \rightarrow$ hadrons*, `arXiv:1207.5031` [hep-ph].

[65] S. Höche, F. Krauss, M. Schönherr and F. Siegert, *QCD matrix elements + parton showers: The NLO case*, `arXiv:1207.5030` [hep-ph].

[66] M. Dasgupta and G. Salam, *Resummation of the jet broadening in DIS*, Eur.Phys.J. **C24** (2002), 213–236, [`hep-ph/0110213` [hep-ph]].

[67] M. Dasgupta and G. P. Salam, *Resummed event shape variables in DIS*, JHEP **0208** (2002), 032, [`hep-ph/0208073` [hep-ph]].

[68] A. Banfi, G. P. Salam and G. Zanderighi, *Resummed event shapes at hadron - hadron colliders*, JHEP **08** (2004), 062, [`hep-ph/0407287` [hep-ph]], Erratum added online, nov/29/2004.

[69] G. Bozzi, S. Catani, D. de Florian and M. Grazzini, *Transverse-momentum resummation and the spectrum of the Higgs boson at the LHC*, Nucl. Phys. **B737** (2006), 73–120, [`hep-ph/0508068`].

[70] G. Bozzi, S. Catani, G. Ferrera, D. de Florian and M. Grazzini, *Production of Drell-Yan lepton pairs in hadron collisions: Transverse-momentum resummation at next-to-next-to-leading logarithmic accuracy*, Phys.Lett. **B696** (2011), 207–213, [`arXiv:1007.2351` [hep-ph]].

[71] D. Amati, A. Bassetto, M. Ciafaloni, G. Marchesini and G. Veneziano, *A treatment of hard processes sensitive to the infrared structure of QCD*, Nucl. Phys. **B173** (1980), 429.

[72] T. Binoth et al., *A proposal for a standard interface between Monte Carlo tools and one-loop programs*, Comput. Phys. Commun. **181** (2010), 1612–1622, [`arXiv:1001.1307` [hep-ph]].

[73] S. Schumann and F. Krauss, *A parton shower algorithm based on Catani-Seymour dipole factorisation*, JHEP **03** (2008), 038, [`arXiv:0709.1027` [hep-ph]].

[74] S. Alekhin et al., *HERA and the LHC - A workshop on the implications of HERA for LHC physics: Proceedings Part A*, hep-ph/0601012.

[75] J.-C. Winter, F. Krauss and G. Soff, *A modified cluster-hadronisation model*, Eur. Phys. J. **C36** (2004), 381–395, [hep-ph/0311085].

[76] F. Krauss et al., *Sherpa's new hadronisation model*, in preparation.

[77] F. Krauss, T. Laubrich and F. Siegert, *Simulation of hadron decays in Sherpa*, in preparation.

[78] M. Schönherr and F. Krauss, *Soft photon radiation in particle decays in Sherpa*, JHEP **12** (2008), 018, [arXiv:0810.5071 [hep-ph]].

[79] H.-L. Lai, M. Guzzi, J. Huston, Z. Li, P. M. Nadolsky et al., *New parton distributions for collider physics*, Phys.Rev. **D82** (2010), 074024, [arXiv:1007.2241 [hep-ph]].

[80] M. Cacciari, G. P. Salam and G. Soyez, *The Anti-k(t) jet clustering algorithm*, JHEP **0804** (2008), 063, [arXiv:0802.1189 [hep-ph]].

[81] M. Cacciari, G. P. Salam and G. Soyez, *FastJet user manual*, Eur.Phys.J. **C72** (2012), 1896, [arXiv:1111.6097 [hep-ph]].

[82] J. A. Maestre, S. Alioli, J. Andersen, R. Ball, A. Buckley et al., *The SM and NLO Multileg and SM MC Working Groups: Summary Report*, arXiv:1203.6803 [hep-ph].

[83] B. Andersson, G. Gustafson, G. Ingelman and T. Sjöstrand, *Parton Fragmentation and String Dynamics*, Phys. Rept. **97** (1983), 31–145.

[84] S. D. Ellis, Z. Kunszt and D. E. Soper, *One-jet inclusive cross section at order α_s^3. Gluons only*, Phys. Rev. **D40** (1989), 2188.

[85] J. R. Andersen and J. M. Smillie, *Constructing all-order corrections to multi-jet rates*, JHEP **1001** (2010), 039, [arXiv:0908.2786 [hep-ph]].

[86] J. R. Andersen and J. M. Smillie, *The Factorisation of the t-channel Pole in Quark-Gluon Scattering*, Phys. Rev. **D81** (2010), 114021, [arXiv:0910.5113 [hep-ph]].

[87] J. R. Andersen and J. M. Smillie, *Multiple Jets at the LHC with High Energy Jets*, JHEP **1106** (2011), 010, [arXiv:1101.5394 [hep-ph]].